J|A|C|S
ARTICLES
Published on Web 03/23/2007

Anharmonic Vibrational Calculations Modeling the Raman Spectra of Intermediates in the Photoactive Yellow Protein (PYP) Photocycle

Adeyemi A. Adesokan,[†] Duohai Pan,[‡] Erick Fredj,[||] Richard A. Mathies,[‡] and R. Benny Gerber*[,†,§]

Contribution from the Department of Chemistry, University of California at Irvine, Irvine, California 92697, Department of Chemistry, University of California at Berkeley, Berkeley, California 94720, Department of Computer Science, Jerusalem College of Technology, Jerusalem 91160, Israel, and Department of Physical Chemistry and The Fritz Haber Research Center, The Hebrew University of Jerusalem, Jerusalem 91904, Israel

Received September 25, 2006; E-mail: benny@fh.huji.ac.il

Abstract: The role of anharmonic effects in the vibrational spectroscopy of the dark state and two major chromophore intermediates of the photoactive yellow protein (PYP) photocycle is examined via ab initio vibrational self-consistent field (VSCF) calculations and time-resolved resonance Raman spectroscopy. For the first time, anharmonicity is considered explicitly in calculating the vibrational spectra of an ensemble consisting of the PYP chromophore surrounded by model compounds used as mimics of the important active-site residues. Predictions of vibrational frequencies on an ab initio corrected semiempirical potential energy surface show remarkable agreement with experimental frequencies for all three states, thus shedding light on the potential along the reaction path. For example, calculated frequencies for vibrational modes of the red-shifted intermediate, PYP_L, exhibit an overall average error of 0.82% from experiment. Upon analysis of anharmonicity patterns in the PYP modes we observe a decrease in anharmonicity in the C_8-C_9 stretching mode ν_{29} (trans−cis isomerization marker mode) with the onset of the cis configuration in PYP_L. This can be attributed to the loss of the hydrogen-bonding character of the adjacent C_9-O_2 to the methylamine (Cys69 backbone). For several of the modes, the anharmonicity is mostly due to mode−mode coupling, while for others it is mostly intrinsic. This study shows the importance of the inclusion of anharmonicity in theoretical spectroscopic calculations, and the sensitivity of experiments to anharmonicity. The characterization of protein active-site residues by small molecular mimics provides an acceptable chemical structural representation for biomolecular spectroscopy calculations.

1. Introduction

Spectroscopic studies of chromophores embedded in proteins can provide detailed information on the interactions between the chromophore and its environment and on the energy landscapes and the dynamics of the processes involved. A system of much interest in this respect is the photoactive yellow protein (PYP) which mediates a negative phototactic response in the phototropic bacterium *Ectothiorhodorspora halophila*[1,2] and also serves as a structural prototype of the PAS domain superfamily.[3−6] PYP is a 125-residue cytosolic photoreceptor containing a 4-hydroxycinnamic acid (4HCA) chromophore which is covalently bound to the side chain of Cys69 through a thiolester linkage.[7,8]

Photoexcitation of PYP elicits a photocycle leading to several spectrally distinct intermediate states.[9] However, since efforts directed toward probing the pathways of conformational change leading to the PYP signaling state has led to different models, a consensus is yet to be reached. For this reason we present here a basic overview of the PYP photocycle at ambient conditions.[10] In the ground state the chromophore PYP_{dark} (or pG) is found in a negatively charged configuration stabilized through a hydrogen-bonding network with Tyr42 and Glu46. Absorption of blue light results in the isomerization of PYP_{dark} from the trans to the cis configuration, in pico- to nanosecond time scales to a red-shifted intermediate PYP_L (or pR or I_1, λ_{max}

[†] University of California, Irvine.
[‡] University of California, Berkeley.
[||] Jerusalem College of Technology.
[§] The Hebrew University of Jerusalem.

(1) Meyer, T. E. *Biochem. Biophys. Acta* **1985**, *806*, 175−183.
(2) Sprenger, W. W.; Hoff, W. D.; Armitage, J. D.; Hellingwerf, K. J. *J. Bacteriol.* **1993**, *175*, 3096−3104.
(3) Kort, R.; Hoff, W. D.; Van West, M.; Kroon, A. R.; Hoffer, S. M.; Van Beeumen, J. J.; Hellingwerf, K. J. *EMBO J.* **1996**, *15*, 3209−3218.
(4) Pellequer, J. L.; Wager-Smith, K. A.; Kay, S. A.; Getzoff, E. D. *Proc. Natl. Acad. Sci. U.S.A.* **1998**, *95*, 5884−5890.
(5) Taylor, B. L; Zhulin, I. B. *Microbiol. Mol. Biol. Rev.* **1999**, *6*, 479 ff.
(6) Anantharaman, V.; Koonin, E. V.; Aravind, L. *J. Mol. Biol.* **2001**, *307*, 1271−1292.
(7) Hoff, W. D.; Dux, P.; Hard, K.; Devreese, B.; Nugteren-Roodzant, I. M.; Crielaard, W.; Boelens, R.; Kaptein, R.; Van, Beeumen, J.; Hellingwerf, K. J. *Biochemistry* **1994**, *33*, 13959−13962.
(8) Baca, M.; Borgstahl, G. E. O.; Boissinot, M.; Burke, P. M.; Williams, D. R.; Slater, K. A.; Getzoff, E. D. *Biochemistry* **1994**, *33*, 14369−14377.
(9) Ujj, L.; Devanathan, S.; Meyer, T. E.; Cusanovich, M. A.; Tollin, G.; Atkinson, G. H.; *Biophysics J.* **1998**, *75*, 406−412.
(10) Cheng, G.; Cusanovich, M. A.; Wysocki, V. H. *Biochemistry* **2006**, *45*, 11744−11751.

10.1021/ja066903v CCC: $37.00

= 480 nm). The observed chromophore isomerization is accompanied by minimal protein conformational changes. In the submicrosecond time scale, PYP_L is transformed initially into a blue-shifted intermediate called I_2 or pB′, (λ_{max} = 370 nm) and a proton is transferred from Glu46 to the chromophore and then finally to the signaling state PYP_M (or $I_{2'}$ or pB , λ_{max} = 355 nm) on a millisecond time scale. This formation of the signaling state PYP_M which is recognized by the partner protein in the signaling cascade is also accompanied by a large conformational change in the protein.[11] Our focus in this study is limited to the three major PYP states and the nomenclature PYP_{dark}, PYP_L, and PYP_M is used to denote the PYP dark state, red-shifted state, and blue-shifted signaling state, respectively.

Extensive and detailed structural analysis has been carried to out on the dark state and two major intermediates of the PYP photocycle, PYP_L and PYP_M. In the case of PYP_{dark} structural characterization has been via both static and time-resolved X-ray diffraction studies in the solid phase[12−14] and also by nuclear magnetic resonance (NMR) in the condensed phase.[15] In addition to these, time-resolved X-ray diffraction methods and step-scan FTIR[16] has been used to elucidate the structure and dynamics of PYP_L and PYP_M. Furthermore, insight into the geometries of PYP intermediates which exist only at an ultrafast time scale have been made available through cryotrap methods,[17−19] UV/vis, vis/IR pump−probe studies, and ultrafast pump−probe absorption and fluorescence spectroscopy methods have been employed.[20−24] Finally, resonance Raman spectroscopy has been used as a means of studying structural changes of the chromophore and interaction with surrounding amino acid residues such as Tyr42 and Glu46.[25−28]

The structure of PYP_M has been found to exhibit significant differences between crystalline form and in solution.[30,31] It has thus been noted that vibrational spectroscopy may provide an advantage over other structural techniques, as it is able to provide crucial insights into the correlation between the PYP spectra and chromophore chemical structure especially during the primary photochemical transitions under a variety of conditions.[32] A very fundamental strength of vibrational spectroscopy is that it contains, in principle, information on the interactions and on the potential energy surfaces of the system. In this respect, the importance of anharmonic couplings is very significant. These couplings govern energy transfer between different modes and other properties that depend on the displacement of the atoms away from equilibrium. A question of major interest is whether the experimental vibrational data are sensitive to the anharmonic interactions and whether a computational treatment that includes these effects is feasible. Recent developments in algorithms for anharmonic vibrational calculations has made it possible to simulate vibrational spectra in large systems.[33−36]

In this work we present the first computational study of the anharmonic vibrational spectroscopy of the three major PYP states in a mimicked environment by means of the vibrational self-consistent field method (VSCF).[36−39] The calculations are for a multidimensional potential energy surface of a semiempirical electronic structure theory, improved by input from relatively high level ab initio calculations. On the basis of lessons from previous calculations for other systems, it is known that the kind of spectroscopic accuracy obtained here cannot be reached with standard empirical forcefields.[27−29] Calculations were carried out on a 4-hydroxycinnamyl methyl thiolester (4HCMT) model of the PYP chromophore dark state and major intermediates influenced by PYP active site amino acid residue mimics.[28,29]

Major progress has also been made with simulations involving molecular dynamics analyses of the initial events following the photoactivation of PYP.[32] However the challenge in this field remains in obtaining good agreement between theoretical prediction and the actually measured dynamical changes in the PYP structure.[32] We believe the key to such an accord between theory and experiments lies in the quality of the potential energy surface used in the simulations. The ultimate test of the forcefield is by comparison with experimental data. This application of anharmonic corrections to the computed PYP vibrational spectra is critical for quantitative comparison with experiment and provides insight into the analysis of existing

(11) Borucki, B.; Devanathan, S.; Otto, H.; Cusanovich, M. A.; Tollin, G.; Heyn, M. P. *Biochemistry* **2002**, *41*, 10026−10037.
(12) Perman, B.; Srajer, V.; Ren, Z.; Teng, T. Y.; Pradervand, C.; Ursby, T.; Bourgeois, D.; Schotte, F.; Wulff, M.; Kort, R.; Hellingwerf, K.; Moffat, K. *Science* **1998**, *279*, 1946−1950.
(13) Ren, Z.; Perman, B.; Srajer, V.; Teng, T. Y.; Pradervand, C.; Bourgeios, D.; Schotte, F.; Ursby, T.; Kort, R.; Wulff, M.; Moffat, K. *Biochemistry* **2001**, *40*, 13788−13801.
(14) Schmidt, V.; Pahl, R.; Srajer, V.; Anderson, S.; Ren, Z.; Ihee, H.; Rajagopal, S.; Moffat, K. *Proc. Natl. Acad. Sci. U.S.A.* **2004**, *101*, 4799−4804.
(15) Dux, P.; Rubinstenn, G.; Vuister, G. W.; Boelens, R.; Mulder, F. A. A.; Hard, K.; Hoff, W. D.; Kroon, A. R.; Crielaard, W.; Hellingwerf, K. J.; Kaptein, R. *Biochemistry* **1998**, *37*, 12689−12699.
(16) Brudler, R.; Rammelsberg, R.; Woo, T. T.; Getzoff, E. D.; Gerwert, K. *Nat. Struct. Biol*. **2001**, *8*, 265−270.
(17) Imamoto, Y.; Shirahige, Y.; Tokunaga, F.; Kinoshita, T.; Yoishara, K.; Kataoka, M. *Biochemistry* **2001**, *40*, 8997−9004.
(18) Genick, U. K.; Soltis, S. M.; Kuhn, P.; Canestrelli, I. L.; Getzoff, E. D. *Nature* **1998**, *392*, 206−209.
(19) Kort, R.; Hellingwerf, K. J.; Ravelli, R. B. G. *J. Biol. Chem.* **2004**, *279*, 26417−26424.
(20) Baltuska, A.; van Stokkum, I. H. M.; Kroon, A.; Monshouwer, R.; Hellingwerf, K. J.; van Grondelle, R. *Chem. Phys. Lett.* **1997**, *270*, 263−266.
(21) Devanathan, S.; Pacheco, A.; Ujj, L.; Cusanovich, M.; Tollin, G.; Lin, S.; Woodbury, N. *Biophys. J*. **1999**, *77*, 1017−1023.
(22) Vengris, M.; van der Horst, M. A.; Zgrablic, G.; van Stokkum, I. H. M.; Haacke, S.; Chergui, M.; Hellingwerf, K. J.; van Grondelle, R.; Larsen, D. S. *Biophys. J*. **2004**, *87*, 1848−1857.
(23) Gensch, T.; Gradinaru, C. C.; van Stokkum, I. H. M.; Hendriks, J.; Hellingwerf, K. J.; van Grondelle, R. *Chem. Phys. Lett.* **2002**, *356*, 347.
(24) Groot, M. L.; van Wilderen, L. J. G. W.; van der Horst, M. A.; van Stokkum, I. H. M.; Hellingwerf, K. J.; van Grondelle, R. *Biochemistry* **2003**, *42*, 10054−10059.
(25) Heyne, K.; Mohammed, O. F.; Usman, A.; Dreyer, J.; Nibbering, E. T. J.; Cusanovich, M. A. *J. Am. Chem. Soc*. **2005**, *127*, 18100−18106.
(26) Kim, M.; Mathies, R. A.; Hoff, W. D.; Hellingwerf, K. J. *Biochemistry* **1995**, *34*, 12669−12672.
(27) Pan, D.; Phillip, A.; Hoff, W. D.; Mathies, R. A. *Biophys. J*. **2004**, *86*, 2374.
(28) Unno, M.; Kumauchi, M.; Sasaki, J.; Tokunaga, F.; Yamauchi, S. *Biochemistry* **2002**, *41*, 5668−5674.
(29) Unno, M.; Kumauchi, M.; Sasaki, J.; Tokunaga, F.; Yamauchi, S. *J. Phys. Chem. B* **2003**, *107*, 2837−2845.
(30) Xie, A.; Keleman, L.; Hendriks, J.; White, B. J.; Hellingwerf, K. J.; Hoff, W. D. *Biochemistry* **2001**, *40*, 1510−1517.
(31) Rubinstenn, G.; Vuister, G. W.; Mulder, F. A. A.; Dux, P. E.; Boelens, R.; Hellingwerf, K. J.; Kaptein, R. *Nat. Struct. Biol.* **1998**, *5*, 568−570.
(32) Hellingwerf, K. J.; Hendriks, J.; Gensch, T.; *J. Phys. Chem. A* **2003**, *107*, 1082−1094.
(33) Adesokan, A. A.; Fredj, E.; Brown, E. C.; Gerber, R. B. *Mol. Phys.* **2005**, *103*, 1505−1520.
(34) Brauer, B.; Gerber, R. B.; Kabelac, M.; Hobza, P.; Bakker, J. M.; Abo Riziq, A. G.; deVries, M. S. *J. Phys. Chem A* **2005**, *109*, 6974−6984.
(35) Barone, V.; Festa, G.; Grandi, A.; Rega, N.; Sanna, N. *Chem. Phys. Lett.* **2004**, *388*, 279−283.
(36) Brauer, B.; Chaban, G. M.; and Gerber, R. B.; *Phys. Chem. Chem. Phys.* **2004**, *6*, 2543−2556.
(37) Chaban, G. M.; Jung, J. O.; Gerber, R. B. *J. Chem. Phys.* **1999**, *111*, 1623−1629.
(38) Matsunaga, N.; Chaban, G. M.; Gerber, R. B. *J. Chem. Phys*. **2002**, *117*, 3541−3547.
(39) Miller, Y.; Chaban, G. M.; Gerber, R. B. *J. Phys. Chem. A* **2005**, *109*, 6565−6574.

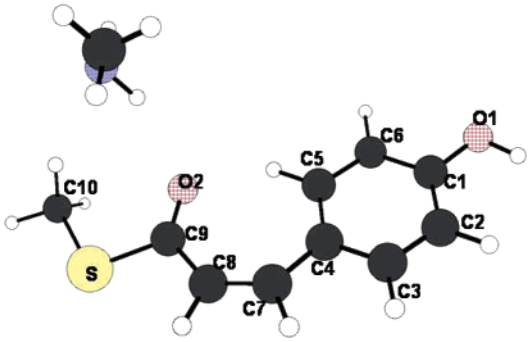

Figure 1. Atom numbering scheme of model of PYP_M (blue-shifted PYP intermediate) with methylamine mimicking the backbone amide of Cys69 used in vibrational frequency calculations.

vibrational spectra, leading to a view of the nature of anharmonicity in the dark state and two intermediate states of PYP. This also provides a basis for proposing inter- and intrachromophore vibrational energy relaxation patterns for PYP.

The outline of this paper is as follows. In the Methods section we present details of experimental methodology, a justification of the theoretical model used in our spectroscopy calculations, and an overview of the VSCF method. In the Results and Discussion section, we present a comparison of theory with experiments, discuss the nature of anharmonic effects in the PYP photocycle, examine the evolution of the PES along the reaction path, and consider the use of mimics. We close with concluding remarks on the importance of accurate anharmonic calculations for understanding spectra and chemical reactions.

2. Methods

2.1. Molecular Mimics. Structural models where used in this study to mimic the PYP chromophore 4HCA and the three crucial protein active site residues Tyr42, Glu46, and Cys69. This was done mainly to reduce the computational cost and feasibility while trying to maintain a reasonably chemically similar environment. This mimic ensemble has been used in a previous study and has been found to give a good representation of the PYP 4HCA chromophore and the important amino acid residues.[28] For the long-lived blue-shifted signaling state intermediate, PYP_M, a protonated chromophore in the form of cis-4-hydroxycinnamyl methyl thiolester (4HCMT) whose carbonyl oxygen forms a hydrogen bond with the amide nitrogen of methylamine; thus mimicking Cys69, was used in our calculations.[28] A numbering scheme of 4HCMT is presented in Figure 1 below. This model is supported particularly by a previous resonance Raman spectroscopy study that indicates the presence of a hydrogen bond at the carbonyl O_2 for PYP_M in solution.[28] This model is also supported by theoretical work by Pan et al. which theoretically distinguishes between the vibrational spectra of pB′ and PYP_M by the inclusion of a Cys 69 mimic to the PYP_M chromophore.[27] The use of additional mimics to represent Tyr 42 and Glu46 might help shed more light on the differences between the vibrational spectra of PYP_M and pB′ however, these additional calculations are beyond the scope of this study.

In representing PYP_{dark} a deprotonated trans HCMT model was used with methanol, acetic acid, and methylamine as mimics for Tyr42, Glu46, and the backbone amide of Cys69, respectively. The mimics were arranged on the basis of the crystal structure of PYP_{dark}.[28,40] The PYP_L structure on the other hand was based on the crystal structure of the cryotrapped intermediate preceding PYP_L.[18] The methanol and acetic acid mimics are arranged here to maintain the hydrogen-bonding network with the phenolic oxygen of the cis HCMT (Figure 2).

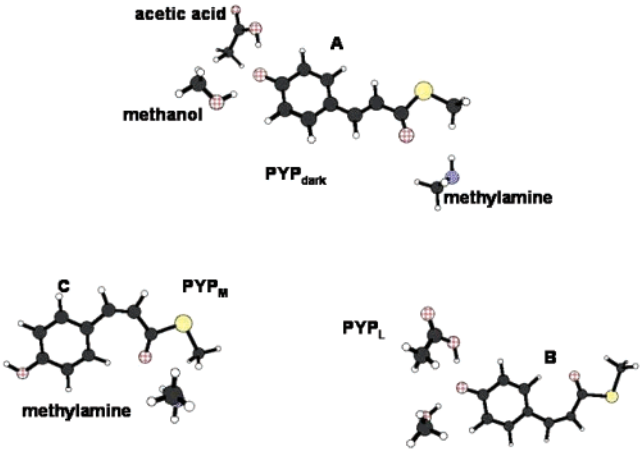

Figure 2. Model of essential amino acid residues surrounding the chromophore intermediates. Methanol−Tyr42, acetic acid−Glu46, methylamine−backbone amide of Cys69

2.2. Potential Functions. Anharmonic vibrational spectroscopy calculations were carried out on an improved semiempirical (PM3) potential energy surface (PES). PM3 is one of several modified NDDO approximation methods (neglect of diatomic differential overlaps methods).[41] Unfortunately however, while computationally efficient, standard PM3 is not sufficiently accurate. Our approach in improving PM3 in this context was originally proposed and implemented for a large range of biomolecules by Brauer et al. and has been validated by subsequent studies.[33−34,36] The method involved changing the harmonic force constants so as to agree with the DFT harmonic force constants obtained using the B3LYP functional[42−43] and the Dunning−Hay double-ζ polarized (DZP) basis[44] as implemented in the GAMESS electronic structure package.[45] That is, the (improved) PM3 is designed to agree with DFT at the harmonic approximation. This is accomplished by introducing a scaling of PM3, such that

$$V_{\text{scaled}}(Q_1, ..., Q_n) = V_{\text{PM3}}(\lambda_1 Q_1, ..., \lambda_n Q_n) \quad (1)$$

where V_{scaled} is a scaled potential, V_{PM3} is the PM3 potential surface, and Q_j is the j normal-mode coordinate. The scale factor λ_i is determined by the ratio

$$\lambda_i = \omega_{\text{DFT},i} / \omega_{\text{PM3},i} \quad (2)$$

where $\omega_{\text{DFT},i}$ is the i harmonic frequency obtained by DFT method, while $\omega_{\text{PM3},i}$ represents the corresponding harmonic frequency obtained by PM3. The λ_j factors were then entered into the potential surface calculation in the VSCF portion of the GAMESS program. Thus, the standard PM3 potential surface in normal coordinates is modified by the scaling of each normal-mode coordinate Q_j by the scale factor λ_j. While the scaling is expected to improve the potential at the harmonic level since DFT should be superior to standard PM3, the effect of the scaling beyond this approximation can only be tested by the predictions obtained with the scaled potential.

The preconditions for carrying out this scaling procedure include similarities in geometries of DFT and PM3 structures and a close correspondence in the nature of the vibrational modes that are being scaled. The proposed scaling makes intuitive sense only if the PM3 normal mode being scaled is similar to the DFT mode used in scaling.

(40) Borgstahl, G. E. O.; Williams, D. R.; Getzoff, E. D. *Biochemistry* **1995**, *34*, 12669−12672.
(41) Stewart, J. J. P. *J. Comp. Chem.* **1989**, *10*, 209−220.
(42) Becke, A. D. *J. Chem. Phys.* **1992**, *97*, 9173.
(43) Becke, A. D. *J. Chem. Phys.* **1993**, *98*, 5643.
(44) Kendall, R. A.; Dunning, T. H.; Harrison, R. J. *J. Chem. Phys.* **1992**, *96*, 6796−6806.
(45) Schmidt, M. W.; Baldridge, K. K.; Boatz, J. J.; Elbert, S. T.; Gordon, M. S.; Jensen, J. J.; Koseki, S.; Matsunaga, N.; Nguyen, K. A.; Su, S.; Windus, T. L.; Dupuis, M.; Montgomery, J. A. *J. Comp. Chem.* **1993**, *19*, 1347−1363.

Table 1. PYP_{dark}−Ground State of the Photoactive Yellow Protein[a]

PM3 mode no.	PM3 (HARM)	DFT (HARM) B3LYP/DZP	harmonic DFT/6311* Pan et al.[27]	VSCF frequency (cm^{-1})	exptl Raman spectroscopy[27]	mode description
26	1778	1557	1501	1523	1530	νC_4-C_3, νC_1-C_2, νC_1-O_1, νC_4-C_7
27	1679	1547	1639	1618	1633	νC_3-C_4, νC_8-C_9, $\nu C_1-C_6-C_5$
29	1657	1607	1525	1608	1558	νC_9-O_2, νC_8-C_9, νC_7-C_8, νC_4-C_7, $\nu C_2-C_3-C_4$
30	1630	1496	1419	1459	1439	νC_5-C_6, νC_2-C_3, νAcetOH
45	1363	1189	1274	1295	1288	νC_1-O_1, νC_4-C_7, νC_8-C_9,$C_2-C_3-C_4$ assym str
47	1332	1361		1307	1302[b]	νC_7-C_8, $C_{10}-H_3$ wag
52	1204	1693	1465	1484	1497	NH_2 wag
54	1185	1068	1146	1173	1163	C−H bending
57	1143	1075	1042	1087	1058	$\nu\nu C_9-O_2$, $\nu\nu C_8-C_9$, $\nu\nu$NH
59[c]	1053	1093		1039	1042	$\nu\nu C_1-O_1$, $\nu\nu$AcetOH
64	1002	847	827	833	827	γ^{γ}ring assym stretch
70	953	1003	977	979	984	$C_{10}-H_3$ twist
71	926	1450	1209	1234	1228	methylamine CH_3 wag
72	918	990	865	901	889	$C_{10}-H_3$ out of plane wag
77	776	764	779	764	767	$\nu\nu C_9$−S, $\nu\nu C_4-C_7$
80	693	750	750	738	732	ring out-of-plane def
83	618	655	655	655	653	C_9-O_2 out-of-plane bend
86	550	543	543	533	538	$\nu\nu C_1-O_1$, $\nu\nu C_9$−S, ring torsion
91	449	424	424	447	447	$\nu\nu C_1-O_1$, $\nu\nu C_1-C_2$, $\nu\nu C_2-C_3$, $\nu\nu C_8-C_9$, νAcet
110	81	99	na	104	104[d]	methanol C═O, str, $\nu\nu C_1-O_1$, $\nu\nu\nu C_8-C_9$, νAcet
108	94	109	na	158	153[d]	methanol C═O, str, $\nu\nu C_1-O_1$, $\nu\nu\nu C_8-C_9$, νAcet
105	155	162	na	179	183[d]	methanol C═O, str, $\nu\nu C_1-O_1$, $\nu\nu C_1-C_2$, νC_8-C_9, νAcet
103	168	182	na	201	202[d]	methanol C═O, str, $\nu\nu C_1-O_1$, $\nu\nu C_1-C_2$, C_2-C_3, νC_8-C_9, $\nu\nu$Acet

[a] Assignment and comparison of theoretical anharmonic frequencies in wave numbers to those obtained from experiments [Pan et al., Chosrowjan et al.];[27,53] ν = stretch, δ = rocking, τ = ring breathing and torsion, γ = out of plane vibration, Acet = acetic acid, na = not available. [b] Reference 17, 28. [c] No harmonic frequencies were assigned to this mode from Pan et al. due to their use of a H_2O mimic instead of a methylamine mode to represent Cys69. [d] Reference 53.

Thus as a test of similarity, a one-to-one correspondence between the normal modes from the two methods (DFT and PM3) are obtained as follows: Initially, the dot products of the normal-mode vectors from PM3 and those from DFT and or MP2/DZP methods are compared to find the most similar modes. Typically an overlap whose absolute value is between 0.6 and 1.0 indicates a likely similarity between normal modes. Next the motions are visually compared using the MacMolPlt program.[46] A visual comparison was required since the direction of the normal-mode vectors is not unique and occasionally, modes involving motions of several types can be similar, yet have partial cancellation.

2.3. The Vibrational Self-Consistent Field Method (VSCF). In this study anharmonic interactions including coupling between different modes are obtained using the VSCF approach and its variants.[38,47] These methods are implemented in the GAMESS suite of codes, and the calculations here used this package. This method can be applied to potential surfaces from electronic structure methods and is reasonably accurate for a variety of systems.[48−49] Unlike analytic forcefields, the potential surface is generated on grid points and is not available as an analytic function. Since VSCF has been discussed extensively in the literature, here we give only a brief overview of the method.[33−34,36−39,48−49]

The VSCF method is used to solve the vibrational Schrondinger equation to obtain vibrational wavefunctions in mass weighed normal coordinates. At the lowest level VSCF is a separable but anharmonic approximation. The vibrational wavefunctions are computed from mean-field potentials that represent the effects of the other vibrations in a given mode.

In practicality, the main computational difficulty in VSCF involves the numerical solution of rather costly multidimensional integrals. We have found it advantageous to represent the potential as a sum of terms that include single-mode potentials $V_j^{diag}(Q_j)$, and interactions between pairs of normal modes $W_{ij}^{coup}(Q_i, Q_j)$. Two types of anharmonic interactions are thus taken into account in the VSCF framework: (1) the intrinsic anharmonicity which is given by the single mode or diagonal potentials and do not involve coupling with other modes and (2) anharmonicity due to mode−mode coupling. Contributions to the potential from interactions of triplets and quartets (or higher order interactions) of normal modes are neglected and the potential is thus written as

$$V(Q_1, ..., Q_N) = \sum_{j=1}^{N} V_j^{diag}(Q_j) + \sum_{i}\sum_{j>i} W_{ij}^{coup}(Q_i, Q_j) \qquad (3)$$

Although this application has proved successful in many cases[33−34,48] it cannot be taken for granted and must be tested for each application.

The simplest separable VSCF approximation may not be of sufficient accuracy for comparison with experiments, and corrections for correlations between different vibrational modes are required. An extension of VSCF using this approach is the correlation corrected VSCF (CC VSCF) method,[47] which includes the nonseparability of the vibrational wavefunction by perturbation theoretic corrections. Another variant of VSCF is the configuration interaction VSCF (VCI VSCF) method, which includes corrections for certain degeneracies between different vibrational modes.[38]

2.4. Experimental Methodology. Photoactive yellow protein was overexpressed in *Escherichia coli* and purified as described[51] except that the histidine-tagged PYP gene was contained in the pQE-80L plasmid transformed into *E. coli* BL21 cells and the cells were lysed by sonication. The Raman measurements were carried out using 100-mM PYP samples in 50 mM sodium phosphate, 100 mM NaCl, pH 7.0 buffer.

Raman measurements for both dark state and PYP_L were performed using the time-resolved Raman microchip flow technique as described

(46) Bode, B. M.; Gordon, M. S.; *J. Mol. Graph. Mod.* **1998**, *16*, 133−138.
(47) Jung, J. O.; Gerber. R. B. *J. Chem. Phys.* **1996**, *105*, 10332−10348.
(48) Gregurick, S. K.; Chaban, G. M.; Gerber, R. B. *J. Phys. Chem. A* **2002**, *106*, 8696−8707.
(49) Benoit, D. M. *J. Chem. Phys.* **2004**, *120*, 562−573.
(50) Xie, A.; Hoff, W. D.; Kroon, A. R.; Hellingwerf, K. J. *Biochemistry* **1996**, *35*, 14671−14678.

Table 2. PYP_L−Red-Shifted Intermediate of the Photoactive Yellow Protein[a]

PM3 mode no.	PM3 (HARM)	DFT harmonic B3LYP/DZP	harmonic DFT/6311[26]	VSCF anharmonic frequency	Raman spectroscopy[26]	mode description
18	1913	1730		1731	1732[b]	$\nu C_9{=}O2$, $C_9{-}C_8$
20	1777	1555	1524	1555	1556	$\nu C{=}C$
22	1677	1657	1670	1657	1666	$\nu C_9{=}O_2$
23	1653	1537	1455	1498	1495	τCC
24	1631	3181	1572	1576	1573	$\nu C_7{-}C_8$, $\nu C_1{-}C_2$, $\nu C_2{-}C_3$
28	1408	1502	1404	1429	1439	methanol $CH_3{-}$Ostr, methanol C−H wag
29	1398	1498		1331	1334[c]	Acet, CH_2 scissor
37	1363	1491		1312	1310[b]	methanol C_3H wag
38	1334	1351	1272	1280	1283	$\nu C{-}O$, $\delta HC_7{=}C_8H$
42	1195	1311	1248	1227	1249	Acet C−OH str, $C_5{-}C_4{-}C_3$ str, C_5H wag
44	1173	1207	1142	1147	1165	ring bend δCH
48	1031	993		962	962[b]	$C_3{-}C_4{-}C_5$ scissors
53	993	1020	1001	990	998	$\nu C_8{-}C_9$
54	976	1005	963	978	979	$\delta HC_7{=}C_8H$
57	951	991		942	943[b]	$C_{10}{-}H_3$ rock
58	927	954	929	886	880	$C_{10}{-}H_3$ twist
60	856	888	859	858	843	$C_9{-}C_8{-}C_7$ symmetric stretch
62	797	790	795	789	762	$HC_7{=}C_8H$ out-of-plane rock, $\nu C_1{-}C_4$
64	764	731	706	741	737	$\nu C_{10}{-}S$
68	669	648		635	642[c]	ring torsion, $\nu C_2{-}C_3$, $\nu C_5{-}C_6$
67	697	746	680	691	667	ring out-of-plane distortion
76	469	480	468	468	461	$\nu C_9{-}S$, $C_9{=}O_2$ ipb

[a] Assignment and comparison of theoretical anharmonic frequencies in wave numbers to those obtained from experiments [Pan et al.];[27] ν = stretch, δ = rocking, τ = ring breathing and torsion, γ = out of plane vibration, Acet = acetic acid. [b] Reference 17. [e] Low-intensity vibration in the Raman spectra. No harmonic frequency was assigned to this mode by Pan et al., ref 27.

Table 3. PYP_M Assignment and Comparison of Theoretical Harmonic Frequencies in Wave Numbers to Those Obtained from Experiments (Unno et al.)[29] [a]

PM3 mode no.	PM3 (HARM)	harmonic DFT/DZP	VSCF anharmonic frequency	Raman spectroscopy[28]	mode description
17	1872	1637	1605	1605	$\nu C_7{=}C_8$
18	1797	1666	1666	1599	$\nu C_7{=}C_8$, νCC
21	1640	1502	1581	1576	νCC, $\nu C_7{=}C_8$
22	1689	1564	1512	1515	νCC, δCH
16	1914	1713	1674	1653	$\nu C_9{=}O_2$
24	1395	1495	1439	1449	$\delta HC_7{=}C_8H$, $\nu CC + \delta CH$
25	1389	1469	1374	1433	$\delta HC_7{=}C_8H$, $\delta HC_7{=}C_8H$
26	1388	1391	1373	1340	$\nu CC + \delta CH$
30	1350	1461	1284	1266	$\delta HC_7{=}C_8H$
32	1303	1371	1308	1330	$\nu CC + \delta CH$, $\delta HC_7{=}C_8H$
33	1241	1358	1174	1174	δCH
35	1195	1311	1311	1290	$\nu C1{-}O$, $\delta HC7{=}C8H$
41	1079	1036	1000	1002	$\nu C_8{-}C_9$
43	1023	1012	982	980	$\gamma HC_7{=}C_8H$
45	985	846	837	837	τCC
51	894	864	864	891	$\delta C_7C_8C_9$
52	861	900	847	855	$\nu C_1{-}O_1$, $\nu C_1{-}C_2$, $\nu C_2{-}C_3$, $\nu C_8{-}C_9$
56	756	729	712	721	$\nu CO + \nu CC$, $\gamma CO + \gamma CH + \gamma CC$, $\gamma C7H$, $\gamma S{-}C_{10}$
58	653	659	637	641	δCCC
59	612	673	660	663	$\gamma C_9{=}O_2$, γC_8H

[a] Theoretical values obtained via PM3 and DFT methods. Frequency assignment is based on visual analysis of vibrational modes; ν = stretch, δ = rocking, τ = ring breathing and torsion, γ = out of plane vibration.

previously.[51] Briefly, a 250 mm cylindrical lens was used to focus the nearly collinear pump (476.5 nm) and probe (413.1 nm) beams to the microprobe image plane. The line images of the beam were subsequently focused by an objective (0.6 NA, 40×) to form displaced ~3 × 100 μm spots in a flowing sample stream. The temporal resolution is determined by adjusting the spatial separation of these two beams and the flowing speed. The Raman spectrum of PYP_{dark} was obtained using just probe-beam excitation. The power of the probe beam is 150 μW, which provides a photoalteration parameter[52] of 0.4, indicating that ~40% of the PYP molecules are photolyzed by the probe beam. For the PYP_L experiment, the pump power of 3.5 mW with a photoalteration parameter of 3.0 was chosen to maximize photolysis of PYP. The flow rate (50 cm/s) and the physical separation (100 μm) between pump and probe beams were chosen to give a 200 μs delay time for detecting Raman scattering from PYP_L.

3. Results and Discussion

3.1. Comparison of Theory with Experiment. The anharmonic vibrational frequencies of the normal modes of vibration

(51) Pan, D.; Mathies, R. A. *Biochemistry* **2001**, *40*, 7929−7936.

(52) Ames, J. B.; Mathies, R. A. *Biochemistry* **1990**, *29*, 7181−7190.

(53) Chosrowjan, H.; Taniguchi, S.; Mataga, N.; Unno, M.; Yamauchi, S.; Hamada, N.; Kumauchi, M.; Tokunaga, F. *J. Phys. Chem. B* **2004**, *108*, 2686−2698.

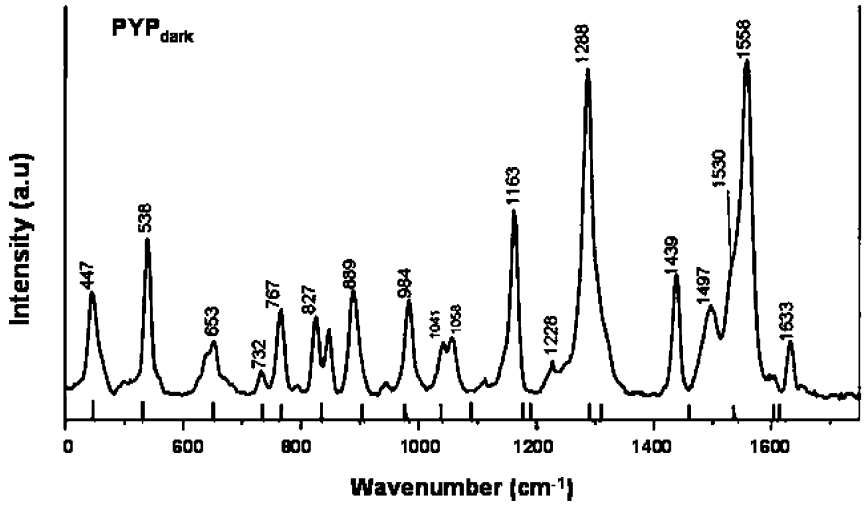

Figure 3. Comparison of VSCF frequencies (short bars) to experimental (Raman) frequencies for PYP dark. (For VSCF results no intensities were used because the VSCF calculation is not yet adapted to include PM3 dipole derivatives for each normal mode.)

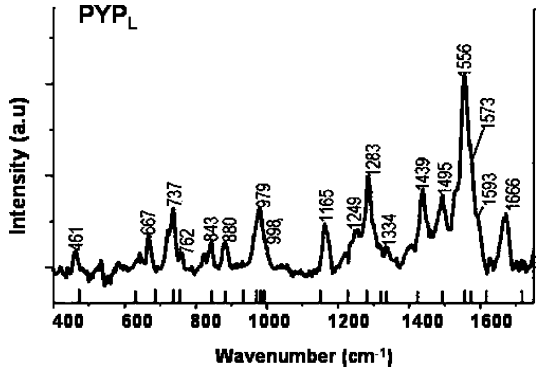

Figure 4. Comparison of calculated VSCF frequencies (short bars) to experimental (Raman) frequencies for PYP_L. (For VSCF results no intensities were used because the VSCF calculation is not yet adapted to include PM3 dipole derivatives for each normal mode.)

of the dark state and two major intermediates of the PYP chromophore in the presence of the mimics were calculated. Tables 1, 2 , and 3 show comparisons of VSCF anharmonic frequencies empirically scaled harmonic frequencies, Raman spectra, and FTIR spectra from previous studies for PYP_{dark}, PYP_L, and PYP_M, respectively. Figures 3 and 4 show comparison of VSCF frequencies to Raman spectra.[26] For all calculated PYP states VSCF anharmonic frequencies compare better to experiment than empirical anharmonic scaling. Empirical anharmonic scaling factors have been used in previous studies to correct the calculated harmonic frequencies for anharmonicity effects.[27−29]

Generally, anharmonic calculations on PYP_L give the best agreement with experiment with a major portion of calculated anharmonic frequencies having a percentage deviation of 1.5% or less from experiment. Furthermore, a total overall average error of 0.82% is observed for this intermediate. Analysis of calculated results for PYP_{dark} shows a major portion of the calculated frequencies with a percentage deviation of less than 1.5% with a total overall average error of 0.92%. In the case of PYP_M most of the percentage deviations are below 4% with a majority of these being under 2%. We believe the reasons for the observed differences can be attributed to the mimics used. Specifically, PYP states which have modes which are heavily dependent on interactions with the chromophore active-site amino acid residues and protein backbone amino acids may not give very accurate results. We believe this is the case with PYP_M which is the longest lived intermediate and also the signaling state of the chromophore. Since this state is correlated with a huge conformational change in the protein, the use of amino acid mimics without the protein backbone might be an unsuitable representation.

In taking a closer look at the agreement of theory to experiment across the PYP dark state and intermediate states, we now focus on four structural marker bands or fingerprint modes which are well characterized by various methods and prominent in each intermediate.

3.1.1. Hydrogen Out-of-Plane (HOOP) Bending Mode. Previous work on retinal proteins has shown that hydrogen out-of-plane (HOOP) vibrations provide a probe of conformational distortion of the chromophore.[54,55] HOOP modes have been used by Pan et al.[27] in characterizing the distortion of the PYP chromophore during the photocycle. The VSCF results have reproduced very well the vibrational frequencies of these HOOP modes in all three PYP states. VSCF results for PYP_L (mode 54) was 978 cm^{-1} compared to experiment at 979 cm^{-1} (Table 2). Experimental frequencies for PYP_{dark} at 984 cm^{-1} (mode 70) was reproduced by VSCF at 979 cm^{-1} (Table 2). The same mode at an experimental frequency of 980 cm^{-1} for PYP_M was reproduced by VSCF at 982 cm^{-1} (mode 43, Table 3). These results point to the advantage of the scaled VSCF method in predicting accurate vibrational frequencies. On visualization these modes are all characterized by the HOOP bending modes which are localized on the $C_7H{=}C_8H$ group.

3.1.2. Protonation State of the Chromophore. The hydrogen bond between the phenolate oxygen O_1 of the chromophore and Tyr42 and the protonated carboxyl group of Glu46, acts in stabilizing the *trans*-PYP configuration as a phenolate ion.[56] Thus, the protonation state marker mode characterized by the C−H bending mode of the chromophore aromatic ring is an

(54) Eyring, G.; Curry, B.; Broek, A.; Lugtenburg, J.; Mathies, R. *Biochemistry* **1982**, *21*, 384−393.
(55) Palings, I.; Pardoen, J. A.; Vandenberg, E.; Winkel, C.; Lugtenburg, J.; Mathies, R. A. *Biochemistry* **1987**, *26*, 2544−2556.
(56) El-Mashtoly, S. F.; Yamauchi, S.; Kumauchi, M.; Hamada, N.; Tokunaga, F.; Unno, M. *J. Phys. Chem. B* **2005**, *109*, 23666−23673.

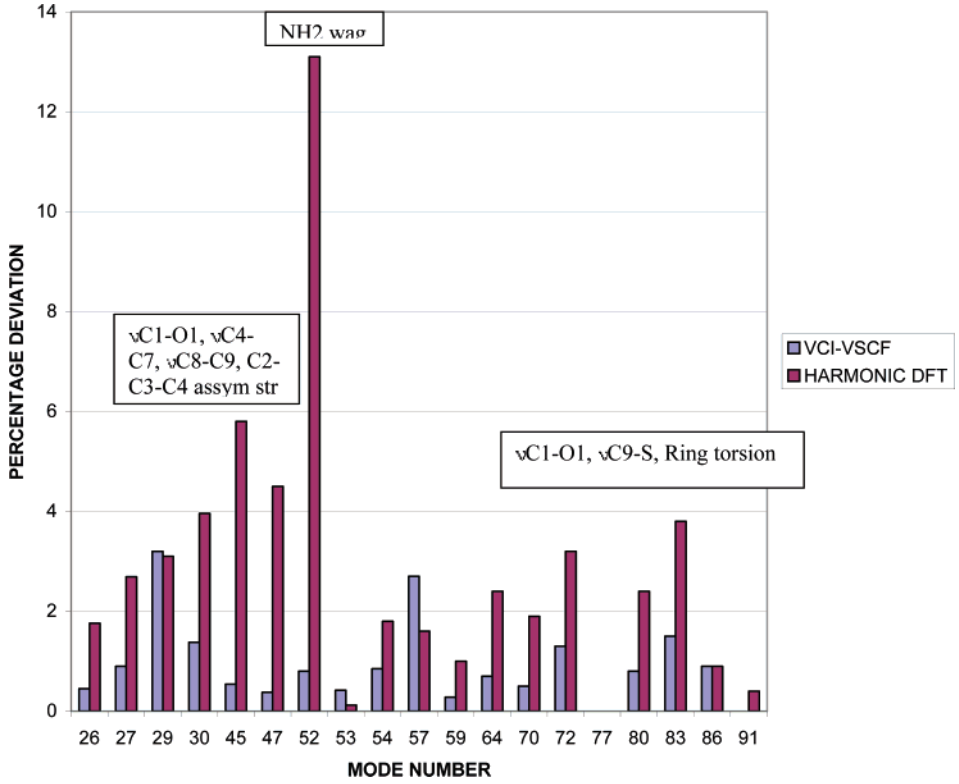

Figure 5. Comparison of percentage deviation of VSCF frequencies of PYP_{dark} and DFT harmonic frequency calculations from experiment.

important indicator of the intermediate state.[16,26,57] Our VSCF calculations predict a value of 1173 cm^{-1} (mode 54, Table 1) as compared to 1163 cm^{-1} in experiments for PYP_{dark}. For PYP_L, VSCF predicts a frequency of 1152 cm^{-1} (mode 44, Table 2) compared to a frequency of 1165 cm^{-1} from Raman spectra experiments.[27] For PYP_M VSCF gives an exact prediction with a frequency of 1174 cm^{-1} (mode 33, Table 3) to 1174 cm^{-1} from Raman spectra experiments.[29] The performance of VSCF gets better relatively for this mode as the residue mimic effect on the chromophore aromatic ring is reduced. The mimic effect is least in PYP_M as the Tyr42 or Glu46 mimics no longer interact with the phenolic oxygen when it becomes protonated.

3.1.3. Trans−Cis Isomerization Mode. Previous work indicates that the frequency of the C_8-C_9 stretching mode depends on trans/cis isomerization around the $C_7=C_8$ bond.[28] Upon photoexcitation of PYP_{dark}, trans/cis isomerization of the $C_7=C_8$ bond takes place producing the PYP_L intermediate. Previous studies have also shown that the C_8-C_9 stretching mode downshifts by ~50 cm^{-1} relative to its frequency in PYP_{dark},[28] marking a cis configuration in PYP_L and PYP_M but a trans form in PYP_{dark}. Scaled VSCF results corresponded exactly for this mode in PYP_L (998 cm^{-1}, mode 53) and were off by 2 cm^{-1} in PYP_M (mode 41, 1000 cm^{-1}). In PYP_{dark} mode 57, VSCF produced a frequency of 1087 cm^{-1} compared to an experimental frequency of 1058 cm^{-1}. The inaccuracy of the predicted frequency in PYP_{dark} may be as a result of limited adequacy of the mimic in representing the protein environment effect.

3.1.4. Chromophore Protein Hydrogen Bond. The $C_9=O_2$ stretching vibration provides an indication of the specific chromophore intermediate state because its' frequency is supposed to be sensitive to hydrogen bonding which in turn varies during the photocycle.[58,27,28] VSCF results for PYP_{dark} mode 29 and PYP_L mode 22 in this mode have a pattern consistent with previous studies and upon visual analysis had vibrational mode displacements in accordance with previous theoretical work. The vibrational frequency of this $C_9=O_2$ stretch is observed to increase from PYP_{dark} to PYP_L by about +40 cm^{-1}. This large shift is due to the loss of the hydrogen bond between the 4HCMT carbonyl oxygen and the hydrogen in the methylamine mimic which represents the backbone amide group of Cys69, as the photocycle proceeds from PYP_{dark} to PYP_L.[27,28] Our observation here is consistent with work by Torii et al.[59] that demonstrates that the C=O stretching frequency of *N*-methyl acetamide is upshifted by about 30 cm^{-1} with the disruption of the H bond.

3.2. Anharmonic Effects. 3.2.1. VSCF and Harmonic Deviations from Experiment. Figure 5 shows a comparison of percentage deviations from experiment for the calculated VSCF and also percent deviation of DFT harmonic frequencies from experiment for PYP_{dark}. Here we see the advantage of VSCF in reducing error in mode 45 (1288 cm^{-1} C−C asymmetric stretch) of this intermediate from a percentage deviation of 5.8% in the harmonic approximation to less than 1% when VSCF is applied. This is also the case for mode 47 (exptl: 1302 cm^{-1}, νC_7-C_8, $C_{10}-H_3$ wag), where the deviation is reduced from 4.2% (harmonic) to about 0.2% (anharmonic). The biggest effect of VSCF in reducing error in PYP_{dark} is seen in mode 52 (exptl: 1497 cm^{-1}, NH_2 wag) where the deviation from experiment is reduced from 13.09% (harmonic) to 0.8%

(57) Unno, M.; Kumauchi, M.; Sasaki, J.; Tokunaga, F.; Yamauchi, S. *J. Am. Chem. Soc.* **2000**, *122*, 4233−4234.
(58) Tonge, P. J.; Carey, P. R. *Biochemistry* **1992**, *31*, 9122−9125.
(59) Torii, H.; Tatsumi, T.; Tasumi, M. *J. Raman Spectrosc.* **1998**, *29*, 537−546.

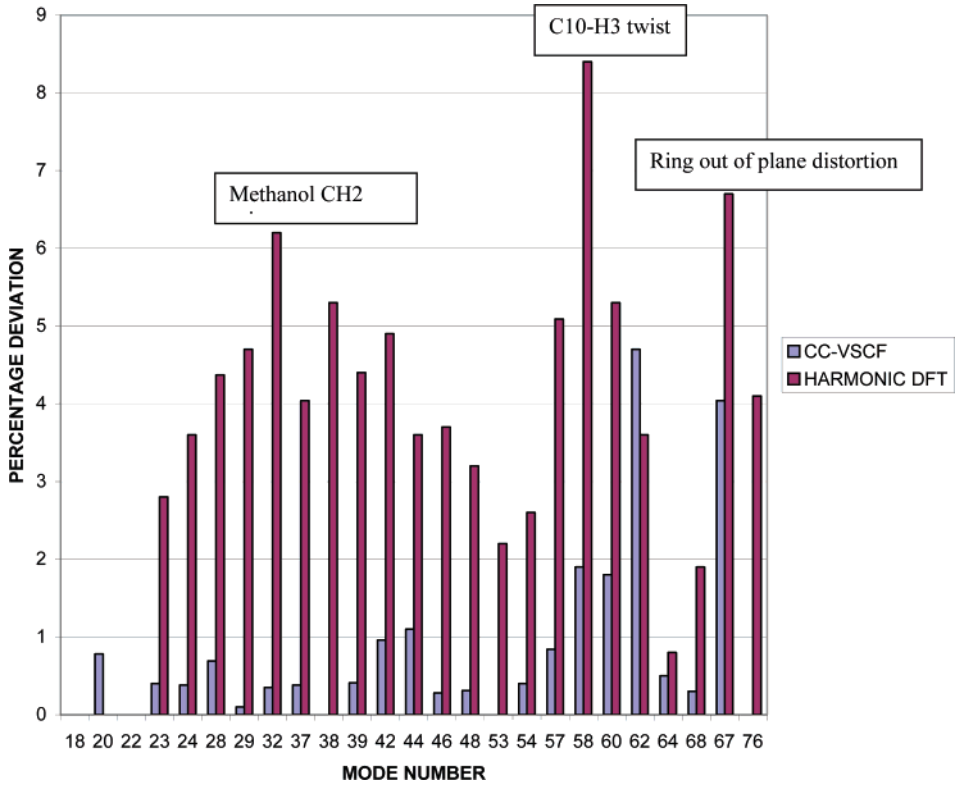

Figure 6. Comparison of percentage deviation of VSCF frequencies of PYP_L and DFT harmonic frequency calculations from experiment.

(anharmonic). The effect of VSCF calculations in reducing large deviations from experimental frequencies due to using a mere harmonic approximation in vibrational spectroscopy calculations is further emphasized in PYP_L mode 76 (expt: 461 cm^{-1}, νC_9-S, $C_9{=}O_2$ ipb) where percentage deviation from experiment is reduced from 4% in the harmonic approximation to 0% in VSCF (see Figure 6). Another case is in mode 38 (expt: 1283 cm^{-1}, $\nu C-O$, $\delta HC_7{=}C_8H$) where error is reduced from 5.2% to 0%. In PYP_M we see a reduction from about 5.8% to 0% in mode 33 (expt: 1174 cm^{-1}). Other examples of VSCF correcting errors are in mode 17 (expt: 1604 cm^{-1}) of PYP_M where percentage deviation from experiment is reduced from 2% to 0% and mode 41 (expt: 1002 cm^{-1}, from 4% to 0%) (Table 3, Figure 7).

3.2.2. Nature of Anharmonic Effects. As mentioned previously, there are two different causes of anharmonic behavior, the intrinsic anharmonicity of the individual modes and the anharmonic coupling between different modes. The contribution of the intrinsic single-mode anharmonicty (ΔE_{diag}) to the frequency is calculated as the difference between the frequency given by the diagonal potential $V_j^{diag}(Q_j)$, and the harmonic value of the frequency; while the contribution of the anharmonic coupling element between modes (ΔE_{coup}) is computed as the difference between the VSCF value and the frequency value given by $V_j^{diag}(Q_j)$. Here we compare values of ΔE_{diag} and ΔE_{coup} for normal modes in each intermediate. For PYP_{dark} the absolute values of ΔE_{diag} is larger than the absolute value of ΔE_{coup}. This indicates that for PYP_{dark} the intrinsic contribution from single-mode anharmonicities is usually greater than the contribution of the anharmonic coupling between the modes. The exception to this observation in PYP_{dark} include, mode 26, mode 30, mode 53, mode 64, and mode 70 (Table 4). The exception here may be due to the spatial arrangement of the atoms in these modes which may lead to greater coupling interaction with other modes. In the case of PYP_L as seen in Table 5, we see typically an equal distribution of the influence of intrinsic and coupled anharmonicity, i.e., modes 18−38. Nearly all the modes in this range have contributions mainly from intrinsic anharmonicity. The lower values on the other hand are mostly dominated by coupled anharmonicity. From mode 42 to mode 76 all but two modes have major contributions from coupled anharmonicity. We see that the signaling state PYP_M is however dominated by intrinsic anharmonicity. Generally we see for PYP_M and PYP_{dark} the absolute value of intrinsic single-mode anharmonicities are larger than the anharmonic coupling between different modes.

Analysis of anharmonicity patterns in the low frequency "trigger" modes and also in fingerprint modes of early stage events like chromophore distortion and trans−cis isomerization show a more important anharmonic mode−mode coupling. Fingerprint modes of later events like chromophore protonation are typified by a stronger intrinsic anharmonicity. Thus we observe that the protonated state, owing to the "loose" binding of the H^+, has high anharmonicity. On the other hand, neutral hydrogen bonding (as in PYP_{dark}) involves strong coupling between the chromophore and mimic modes. The anharmonic mode−mode coupling that characterizes the trans−cis isomerization mode implies an efficient vibrational energy transfer between modes.

An increase in intrinsic anharmonic characteristics is observed from the PYP_L to the PYP_M state for the protonation mode. We propose that the effects which cause a change in protonation state of the chromophore has a lot of intrinsic anharmonic character. For the C_8-C_9 stretching mode ν_{29} (trans/cis isomerization marker mode) a decrease in anharmonicity is seen with the onset of the cis configuration in (PYP_L)

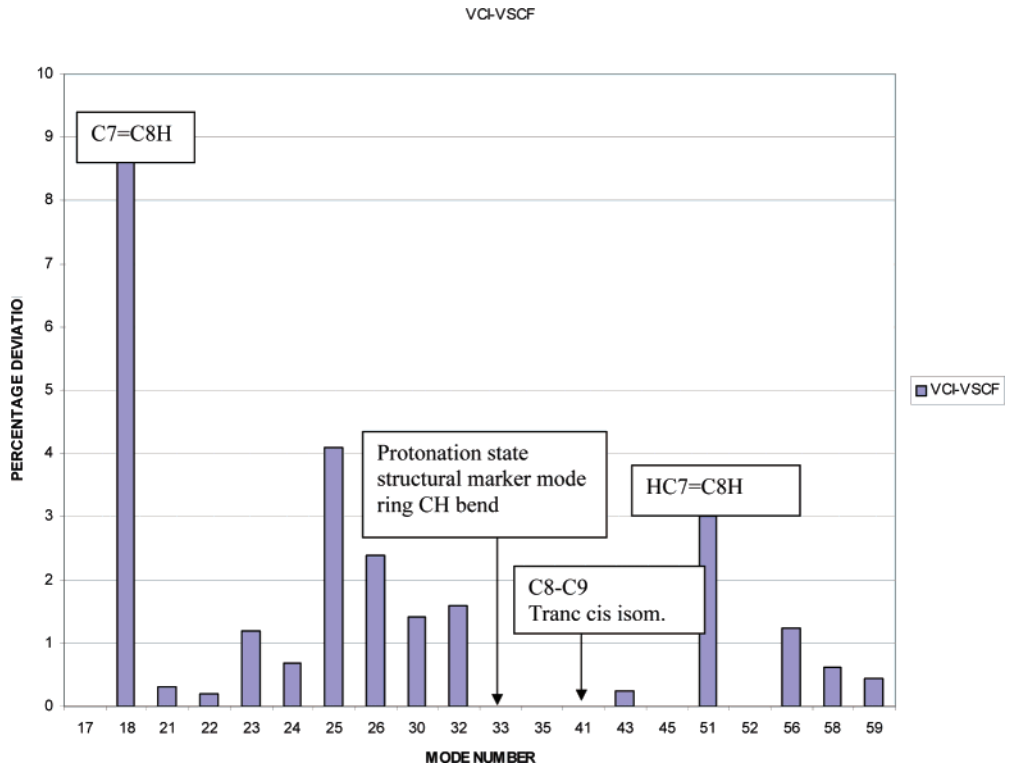

Figure 7. Comparison of percentage deviation of VSCF frequencies of PYP_M from Raman frequencies.

Table 4. PYP_{dark} Comparison between ΔE_{diag} (in cm^{-1}) and ΔE_{coup} (in cm^{-1})

PM3 mode	DFT (HARM)	diagonal frequency	VSCF frequency	expt Raman	ΔE_{diag}	ΔE_{coup}
26	1557	1543	1523	1530	−14	−20
27	1547	1647	1618	1633	100	−29
29	1607	1626	1608	1558	19	−18
30	1496	1480	1459	1439	−16	−21
45	1189	1338	1295	1288	149	−43
47	1361	1333	1307	1302	−28	−26
52	1693	1513	1484	1497	−180	−29
53	1179	1176	1186	1181	−3	−10
54	1068	1167	1173	1163	99	+6
57	1075	1125	1087	1058	50	−58
59	1093	1047	1039	1042	−46	−8
64	847	844	833	827	−3	−11
70	1003	997	979	984	−6	−18
71	1450	1237	1234	1228	−213	−3
72	990	928	901	889	−62	−27
77	764	749	764	767	−15	15
83	750	732	738	732	−18	−6
86	764	749	764	767	−15	15
91	750	732	738	732	−18	−6
110	99	83	104	104	−16	21
108	110	145	158	153	35	13
105	163	162	179	183	−1	17
103	182	191	201	202	9	10

Table 5. PYP_L Comparison between ΔE_{diag} (in cm^{-1}) and ΔE_{coup} (in cm^{-1})

PM3 mode	DFT (HARM)	diagonal frequency	VSCF frequency	expt Raman	ΔE_{diag}	ΔE_{coup}
18	1730	1738	1731	1732	−14	−7
20	1555	1534	1555	1556	−21	21
22	1677	1644	1677	1666	−33	33
23	1537	1518	1498	1495	−19	−20
24	3181	1598	1576	1573	−1583	−22
28	1502	1454	1429	1439	−48	−25
29	1498	1365	1331	1334	−133	−34
37	1491	1339	1312	1310	−152	−27
38	1351	1323	1280	1283	−283	−43
42	1311	1273	1227	1249	−38	−46
44	1207	1173	1147	1165	−34	−26
48	993	980	962	962	−13	−18
53	1020	1013	990	998	−7	−23
54	1005	992	978	979	−13	−14
57	991	986	942	943	−5	−44
58	954	931	886	880	−23	−45
60	888	866	858	843	−22	−8
62	790	799	789	762	9	−10
64	731	746	741	737	15	−5
68	648	651	635	642	3	−16
67	746	688	691	667	−58	−3
76	480	469	468	461	−11	−1

which can be attributed to the loss of the hydrogen-bonding character of the adjacent C_9-O_2 to the methylamine (Cys69 backbone).

3.2.3. Magnitudes of Anharmonic Coupling Between the Modes. Anharmonic coupling between modes has an effect on the frequencies and may play a role in vibrational energy flow.[60] This effect happens to be paramount in a system such as PYP which is characterized by pronounced conformational changes. An analysis of coupling patterns in PYP could provide insight into the origin of conformational changes in the PYP photocycle. Thus, the average absolute value of the coupling potential was studied for the three PYP states. The average coupling potential was plotted over the range of normal-mode coordinates for selected modes in each intermediate (Figure 8). Generally we observe that coupling is nondemocratic.

A very strong coupling between PYP_{dark} mode 57 (expt: 1058 cm^{-1}, νC_9-O_2, νC_8-C_9, νNH) is observed with the methylamine mimic and also the acetic acid mimic. The strong coupling observed is partially due to the hydrogen bonding between the methylamine mimic and the chromophore C9−O2

(60) Leitner, D. *J. Phys. Chem. A* **1997**, *101*, 547−548.

Table 6. PYP_M Comparison between ΔE_{diag} (in cm^{-1}) and ΔE_{coup} (in cm^{-1})

PM3 mode	DFT (HARM)	diagonal frequency	VSCF frequency	Lit. B N_2 matrix	ΔE_{diag}	ΔE_{coup}
17	1637	1620	1605	1605	−17	−15
18	1666	1759	1666	1599	93	−93
21	1502	1606	1581	1576	−1481	−25
22	1564	1532	1512	1515	−157	−20
16	1713	1683	1674	1653	−30	−9
24	1495	1438	1439	1449	−57	1
25	1469	1357	1374	1433	−112	17
26	1391	1377	1373	1340	−14	−4
30	1461	1324	1284	1266	−137	−40
32	1371	1335	1308	1330	−36	−27
33	1358	1227	1174	1174	−131	−53
35	1311	1189	1311	1290	−122	122
41	1036	1022	1000	1002	−14	−22
43	1012	1004	982	980	−8	−22
45	846	843	837	837	−3	−6
51	864	868	864	891	4	−4
52	900	848	900	885	−52	52
56	729	715	712	721	−14	−3
58	659	646	637	641	−13	−9
59	673	656	660	663	−17	−4

(Figure 8). The observed strong coupling with the acetic acid is also due to the hydrogen bonding with the phenolic oxygen on the chromphore and the carboxyl hydrogen. This strong coupling character indicates an efficient vibrational energy transfer from the Cys69 to Glu46 and vice-versa through the chromophore as an energy conduit. This is not the case for PYP_{dark} mode 54 and mode 27 in which a lot of low-intensity coupling with other modes is observed. This result is in agreement with Table 4 which shows mode 57 has a higher absolute ΔE_{coup} value compared to mode 54 and 27.

For PYP_L mode 20 (expt: 1556 cm^{-1}), most of the coupling is observed with modes in close geometric vicinity (Figure 9). The relatively strong uniform coupling observed between the normal modes here might be due to the similarity between the main atom displacements. As mentioned earlier, PYP_M is mostly characterized by intrinsic anharmonicity. We find most of the coupling from PYP_M mode 41(expt: 1002 cm^{-1}, C_8-C_9 stretch) is transferred to the C_8-H stretch, C_9-O_2 stretch and C_7-C_8 stretch modes. Most of the coupling of the PYP_M mode 35 (CH out of plane bending) is found in the C_5H and C_1-O_1 stretch modes.

3.3. Evolution of the Potential along the Reaction Path. Generally, we observe for all three PYP states that calculated anharmonic frequencies for fingerprint modes that are not heavily dependent on mimics show the least deviation from experiment. Calculations for the PYP_M protonation state marker mode (mode 33, 1174 cm^{-1}) which is not dependent on mimics show an exact prediction. Similarly, exact predictions for the trans−cis isomerization fingerprint mode (νC_8-C_9) were observed for PYP_L (mode 53, 998 cm^{-1}) and PYP_M (mode 41, 1000 cm^{-1}) but not for PYP_{dark}. This may be due to a better placement of the Cys69 (methylamine) mimic in PYP_M compared to that in PYP_{dark}. The HOOP mode ($\gamma HC_7{=}C_8H$) is very accurate for all three intermediates as this mode does not require any mimics and is relatively localized.

As the photocycle progresses we see a change in percentage anharmonicity for the fingerprint modes in PYP_{dark}, PYP_L, and PYP_M. For the HOOP mode which is an indicator of chromphore distortion, a steady increase in percentage anharmonicity is observed from PYP_{dark} to PYP_M. Total percentage anharmonicity is 1.93% in PYP_{dark}, 2.7% in PYP_L and 3.05% in PYP_M. The increase in anharmonicity could be attributed to increased chromophore distortion as the photocycle proceeds. For the case of the protonations state marker mode a total percentage anharmonicity of 5.7% is observed in PYP_M, 4.7% in PYP_L, and 1% in PYP_{dark}. The highest anharmonicity for this fingerprint mode is seen in PYP_M. As mentioned previously the high anharmonicity in this mode in PYP_M may be due to the "loose" binding of the H^+. The percentage anharmonicity for the trans−cis isomerization fingerprint mode was 3.6% in PYP_M, 2.2% in PYP_L, and 5.1% in PYP_{dark}. In summary we see that anharmonic effects on PYP modes are not uniform along the reaction path.

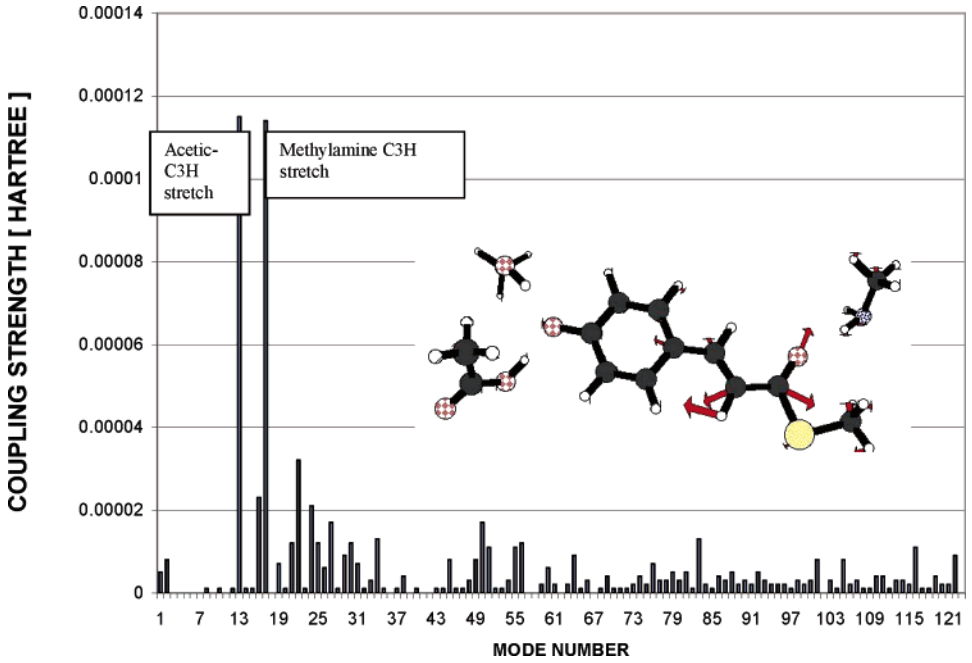

Figure 8. Graph showing integrated coupling potential between PYP_{dark} mode 57 (νC9−O2, νC8−C9, νNH) and other modes.

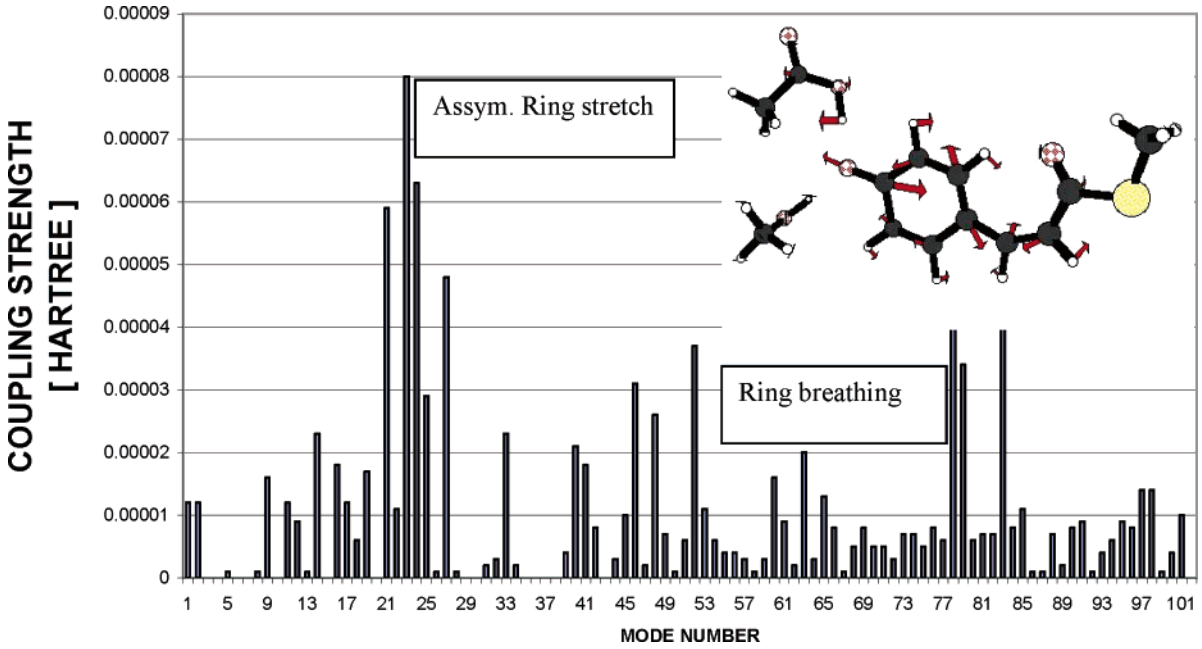

Figure 9. Graph showing integrated coupling potential between PYP_L mode 20 (C−C aromatic stretch) and other modes.

3.4. Molecular Mimics. Specific reasons for the observed differences in accuracy can be attributed to the use of mimics, the importance of which varies for each intermediate. Concerning the use of mimics the following observations are made: Molecular mimics as used here generally represent molecular spectroscopy well. This finding supports earlier work by Unno et al. specifically describing PYP spectroscopy in the presence and absence of mimics.[28] PYP_M with the least use of mimics is shown to have the highest error value. PYP_{dark} with the most use of mimics has a comparatively lower error while, PYP_L with two mimics has the least error. Molecular mimics without a supporting protein backbone may not adequately reproduce chromophore frequencies which are heavily dependent on interactions with protein amino acids. For PYP_M mode 33 (1174 cm^{-1} δCH) (which is not dependent on the protein backbone) we see an increase in accuracy of VSCF since the need for mimicking is reduced. The error in the description of the C−C, C═C stretching mode in PYP_M mode 18 (expt: 1599 cm^{-1}) might be due to the incorrect placement of the methylamine (Cys69 mimic) in PYP_M as optimal placement of this mimic is not yet known. The corresponding modes in PYP_L (mode 20, 1556 cm^{-1}) and PYP_{dark} (mode 26, 1153 cm^{-1}) are well described since this mode in these intermediates is not influenced directly by methylamine (Cys69). We conclude from the use of mimics that the presence of hydrogen bonding between the Cys69 backbone and O_2 may serve to maintain PYP in a protonated state.

4. Concluding Remarks

We have calculated the anharmonic vibrational spectra of the 4HCA PYP chromophore in an active-site mimic environment and comparison between theory and experiment for this system of considerable complexity shows good agreement. For the first time, such a (anharmonic) comparison is done not only for a stable state (PYP_{dark}), but also for two major intermediate states, PYP_M and PYP_L, providing a glimpse into the evolution of the potential along the photocycle. The theoretical−experimental analysis shows that the explicit inclusion of anharmonic effects is very important for achieving agreement between theory and experiment and that experiments are indeed sensitive to anharmonicity. This agreement also implies that the potential used here is reasonable and encourages other applications. In addition, we have noticed that both intrinsic and coupling anharmonic effects are important. Particularly, the trans−cis isomerization modes show a more important anharmonic mode−mode coupling implying an efficient vibrational energy transfer between the modes. On the other hand, fingerprint modes of later stage events like chromophore protonation are typified by a stronger intrinsic anharmonicity. This work shows that the use of carefully chosen mimics makes possible good spectroscopy calculations of complex systems. However, our results also show that it would be useful to develop "clever" mimics that have optimal placements at each stage along the reaction pathway.

Acknowledgment. Assistance from Dr. Masashi Unno in the initial phase of the project is cordially appreciated. We are grateful to Dr. Eric C. Brown for helpful discussions and Dr. B. Brauer for suggestions and for kindly providing the ab-inito scaling code. We also acknowledge Elad Segev for insightful comments on chromophore protonation and other issues. The research at the Hebrew University of Jerusalem was supported by the US-Israel Binational Science Foundation (Grant BSF 2004009). Partial support for this work was also provided by DFG-Germany through Project SFB-450. D.P. and R.A.M. were supported in part by NIH Grant EY-02051.

Supporting Information Available: Summary of bond length comparisons. This material is available free of charge via the Internet at http://pubs.acs.org.

JA066903V